NASA TM X-158

TECHNICAL MEMORANDUM
X-158

FREE-FLIGHT INVESTIGATION OF STATIC STABILITY AND DRAG OF MODELS OF THE SECOND AND THIRD STAGES OF THE HEMISPHERE-NOSED X-17 AT MACH NUMBERS FROM 4 TO 10

By Robert J. Carros

Ames Research Center
Moffett Field, Calif.

CLASSIFIED DOCUMENT - TITLE UNCLASSIFIED

This material contains information affecting the national defense of the United States within the meaning of the espionage laws, Title 18, U.S.C., Secs. 793 and 794, the transmission or revelation of which in any manner to an unauthorized person is prohibited by law.

NATIONAL AERONAUTICS AND SPACE ADMINISTRATION

WASHINGTON February 1960

[redacted]

NATIONAL AERONAUTICS AND SPACE ADMINISTRATION

TECHNICAL MEMORANDUM X-158

FREE-FLIGHT INVESTIGATION OF STATIC STABILITY AND DRAG OF MODELS OF THE SECOND AND THIRD STAGES OF THE HEMISPHERE-NOSED X-17 AT MACH NUMBERS FROM 4 TO 10*

By Robert J. Carros

SUMMARY

Static-stability and drag characteristics of the second and third stages of the X-17 hemisphere-nosed research test vehicle were determined from limited tests of small-scale free-flight models. Coefficients of total zero-lift drag and effective pitching-moment-curve slope were determined from time, distance, and attitude records for the third-stage model at Mach numbers of approximately 4 and 9.6, and for the second-stage model at a Mach number of approximately 8.6. In addition, effective values of pitching-moment-curve slope, normal-force-curve slope, and center-of-pressure location were determined for the second-stage model at a Mach number of 5.5. Effective pitching-moment-curve slope coefficients were also determined at a Mach number of 4.6 for a model made hypersonically similar to the third-stage configuration at a Mach number of 13.8.

It was found that the static stability of the third-stage configuration decreased considerably for a change in Mach number from 4 to 10 and also decreased pronouncedly with decreasing pitching amplitude. This configuration was indicated by the tests to be unstable near zero angle of attack at a Mach number of 9.8. The static stability of the second-stage configuration was also found to decrease with increasing Mach number but to a lesser extent than the third stage. No attempt was made to take account of the observed variation of pitching-moment-curve slope with pitching amplitude other than to consider an effective linear moment-curve slope as a function of maximum amplitude of pitch.

*Title, Unclassified

[redacted]

[redacted]

INTRODUCTION

Ross and Dorrance (ref. 1) were perhaps the first to suggest that a cone-frustum or flare at the rear of a body would offer a means of providing stability at high speeds. Since that time only a relatively small amount of data had been obtained on the stability of this type of body-flare configuration. For the most part, the data available were limited to bodies such as cone-cylinders stabilized by flares and to Mach numbers below 4. (An analysis and correlation of available data of this kind has been made recently in ref. 2.) The lack of sufficient information with regard to the size and geometry of the minimum flare that would stabilize a wingless configuration at very high speeds was apparent when the Lockheed Aircraft Corporation undertook the preliminary design of the X-17 re-entry test vehicle. The X-17, a blunt-nosed body of revolution, was intended to fly at Mach numbers up to 15. The present investigation was conducted to provide preliminary data on the stability of the second and third stages of the X-17 hemisphere-nosed configuration. These tests were conducted at Mach numbers between 4 and 10 in the Ames supersonic free-flight wind tunnel and range.

A 1 9 0

NOTATION

A	reference area, $\frac{\pi d^2}{4}$, sq ft
$C_{D_{\alpha=0}}$	total zero-lift drag coefficient
C_{m_α}	effective pitching-moment-curve slope coefficient, $\left(\frac{2\pi}{\lambda}\right)^2 \frac{2I}{\rho A l}$, per radian
C_{N_α}	effective normal-force-curve slope coefficient, per radian
d	third-stage cylinder diameter, ft
I	moment of inertia about lateral axis through model center of gravity, slug-ft^2
l	model length, ft
M	Mach number based on free-stream properties
R	Reynolds number based on free-stream properties and model length
T	free-stream static temperature, $^\circ R$
x	model distance traveled relative to air stream from point of first observation, in.

[redacted]

X_{cg} distance from model nose to center-of-gravity position, ft

X_{cp} distance from model nose to effective center-of-pressure position, ft

α angle of attack, measured between model axis and flight path, deg

α_{max} maximum amplitude of pitching oscillation, deg

λ distance traveled by model, relative to air stream, in one cycle of pitching motion, ft/cycle

ρ free-stream air density, slugs/cu ft

PROCEDURE AND TEST TECHNIQUE

Stability data were obtained from free-flight tests of small-scale models of the X-17 research test vehicle propelled from smooth-bore guns of 20mm and 1-3/4-inch bore size. The models were flown both in still air in the Ames underground ballistic range to give resultant nominal Mach numbers of 4 and 4.6, and upstream through the Mach number 3 air stream of the Ames supersonic free-flight wind tunnel (ref. 3) to give resultant nominal test Mach numbers of 5.5, 8.6, and 9.6. During each flight a time, distance, and attitude record was obtained from which total drag, and effective values of pitching-moment-curve slope, normal-force-curve slope, and center-of-pressure location were determined where possible. The wind-tunnel test section contains nine shadowgraph stations at 3-foot intervals, each of which provides a side view and a plan view shadowgraph. The underground ballistic range is instrumented with seven shadowgraph stations at 11-foot intervals, each providing a side view and a plan view shadowgraph. This facility uses data-recording equipment which is essentially equivalent to that used in the wind-tunnel facility, and the test technique and data reduction are basically the same.

The test models, shown in figures 1 and 2, had configurations closely similar to the X-17 test vehicle with a hemispherical nose. In addition, a "hypersonically similar" model of the third stage was tested at a Mach number of 4.6 to simulate a Mach number of 13.8. The body was foreshortened in relation to its diameter in the ratio of 3:1, except for the nose which remained hemispherical.

The models were constructed of 7075-T6 aluminum alloy with tungsten-steel alloy and magnesium as ballast materials. The nominal center-of-gravity locations obtained are indicated in the figures. The models were launched from smooth bore guns with the aid of sabots such as the one shown in figure 2.

The tests were carried out at various Mach numbers, Reynolds numbers, and free-stream static temperatures. Nominal values of these conditions are shown in the following table.

Number of rounds	Conditions			
	Model	M	R, $\times 10^{-6}$	T, $^{\circ}R$
1	Third stage	4	7.3	530
4	Third stage	9.6	8.9	190
3	Second stage	5.5	10.9	190
2	Second stage	8.6	16.4	190
3	Hypersonically similar third stage	4.6	8.0	530

A detailed discussion of the calculation procedures used to determine the aerodynamic coefficients is given in references 3 and 4. Basically, the static stability is obtained from the observed pitching frequency, and the drag from the observed deceleration, both of which are computed from the shadowgraph-chronograph record of the model position-time history. The stability as reported herein was reduced assuming linearity of the pitching-moment curve. The proper use of the data obtained from this assumption will be discussed under Results.

RESULTS AND DISCUSSION

Tests of the Third-Stage Model

Figure 3 is an example of the basic data obtained from the shadowgraphs. Angle of attack is plotted as a function of distance flown for two rounds at a Mach number of 9.6. In these examples approximately 1/4 cycle of motion occurred, but in flights with other models and at other test conditions, observation of as much as 1-1/2 cycles of motion occurred, this depending on the dynamic pressure, margin of aerodynamic stability, and model inertia. From the basic data, values of C_{m_α} are calculated by means of the following equation, derived for linear variation of C_m with α.

$$C_{m_\alpha} = \left(\frac{2\pi}{\lambda}\right)^2 \frac{2I}{\rho A l} \qquad (1)$$

Since the terms I, ρ, A, and l in equation (1) were, for the two rounds of figure 3, nominally equal, an interesting result appears. The wave lengths shown in the figure are plainly different, and therefore C_{m_α} will be different. Consequently, C_{m_α} was correlated as a function of maximum pitching amplitude[1] as shown in figure 4; the results indicate a strong dependence of the effective C_{m_α} upon pitching amplitude. Linear extrapolation of the line connecting the two points in figure 4 indicates that the model would be unstable near a maximum pitching amplitude of 2°.

No attempt was made to account for the observed variation of C_{m_α} with pitching amplitude other than to plot an "effective" C_{m_α} as a function of α_{max} as in figure 4. This effective C_{m_α} is the value obtained from equation (1) using the observed wave lengths. This information can be applied to the full-scale missile by reversing the procedure; that is, the pitching frequency can be obtained as a function of the maximum pitching amplitude by the use of the coefficients of figure 4. The effective stability will, at a given amplitude of pitching, depend on whether the oscillation (with respect to earth-fixed axes) is planar or elliptical. For a planar oscillation the value of effective C_{m_α} determined would be an average value for the amplitude range between $\alpha = 0$ and $\alpha = \alpha_{max}$. For an elliptical oscillation, the effective C_{m_α} determined would be an average value for the amplitude range between $\alpha > 0$ and $\alpha = \alpha_{max}$. It is important to note, therefore, that for all of the results presented the oscillations were very nearly planar, being thin ellipses with minor to major axis ratios of approximately 1 to 8.

The variation of C_{m_α} with Mach number for the third-stage configuration is shown in figure 5. The pitching amplitudes are indicated. The effect of Mach number on static stability (for the small angle range) is seen to be considerable, C_{m_α} changing from -0.64 at $M = 4$ to 0 (indicating neutral stability) at $M = 9.8$ for the models with $X_{cg}/l = 0.537$. (Neutral stability was observed in this flight from a linear variation of α with x, indicating that the pitching moment was zero in the range from 0° to 3°.) It is interesting to note that the inability of the model to stabilize at small pitching amplitudes and Mach numbers in excess of 10 was later found to be characteristic of the full-scale model (e.g., refs. 5 and 6).

The increase in static stability with increasing angle of attack shown in figure 4 may be qualitatively explained in terms of the strong bow shock wave produced by the blunt nose of the body. For the model at low angle of attack, the air acting on the flare has passed through the strong segment of the bow shock wave at the model nose, which considerably

[1]The pitching implitude for a given round is a random quantity and depends on disturbances imparted to the model upon leaving the gun muzzle.

reduces the dynamic pressure at the flare. At high angles, however, the air striking the flare on the windward side of the model passes through a weaker segment of the bow shock wave which correspondingly causes less reduction in dynamic pressure. This net increase in dynamic pressure at high angles is believed to be responsible for the increase in static stability with increasing angle of attack.

Similarly the loss in static stability with increasing Mach number shown in figure 5 may also be qualitatively explained in terms of the strong bow shock wave. This strong bow shock wave is responsible for a large loss in dynamic pressure across the wave and this loss increases as the Mach number is increased. Since the flare is operating in this region of rapidly decreasing dynamic pressure with increasing Mach number, it loses its effectiveness as Mach number is increased.

Figure 6 shows the level of total zero-lift drag coefficient for the two test Mach numbers of approximately 4 and 9.5. Also shown in figure 6, reproduced from reference 7, is the total drag coefficient (approximately 98-percent wave drag) contributed by the hemispherical nose of the body. The major portion of the remaining drag then is contributed by the flare. Since the drag of the sphere is essentially constant at all Mach numbers, the decrease in drag coefficient with increasing Mach number shown in the figure is a result of a decrease in the flare drag coefficient. This decrease is consistent with the decrease in dynamic pressure with increasing Mach number behind the bow shock wave and with the decrease in stability as discussed earlier.

Tests of the Second-Stage Model

The testing of the second-stage model was confined chiefly to Mach number 5.5 and the pitching amplitudes obtained were small, between 2.5° and 3.0°. At this Mach number effective values of C_{m_α}, C_{N_α}, and X_{cp}/l were obtained. In addition an effective value of C_{m_α} was determined at a Mach number of 8.6 from a round with a maximum pitch amplitude of 13.8°. A value of zero-lift drag coefficient was also obtained at a Mach number of 8.4 and a pitch amplitude of less than 1°.

The pitching-moment data for both Mach numbers are shown in figure 7. At a Mach number of 5.5, three models with different center-of-gravity positions were tested and the data are plotted against X_{cg}/l. From this plot, the center-of-pressure location was found (by extension of the curve to the point of neutral stability) to be at the 73-percent point of body length. The slope of this curve is the effective C_{N_α} and is equal to 18.2 per radian.

The one value of C_{m_α} for a Mach number of 8.6 is shown by the flagged symbol and fell about 25 percent below the curve for Mach number 5.5 even though the pitching amplitude was much larger at the higher Mach number. This decrease in stability with increasing Mach number is similar to that experienced with the third-stage model although not as severe because the ratio of blunt-nose diameter to base-flare diameter is less for the second stage and also because of the higher pitching amplitude obtained in the one test at the higher Mach number (see above discussion of fig. 4).

The drag coefficient for a round at $M = 8.4$ is plotted in figure 6 and shows a slight increase over an interpolated value for the third stage. The increase represents principally the pressure drag of the second flare.

Some wind-tunnel static stability and drag data are presented in reference 8 on a configuration similar to (but not identical to) the second-stage models of the present test. The drag coefficient from the reference 8 test is approximately 1.24 at a Mach number of 6.86 compared to 1.25 at a Mach number of 8.4 for the results of the present investigation. However, the average value of C_{m_α}, obtained from figure 17 of reference 8 in the angle-of-attack range from 0° to 3°, is approximately a factor of 2-1/2 times greater than the C_{m_α} obtained in this investigation (fig. 7). This increase in C_{m_α} may be attributed, in part at least, to the lower Reynolds number of the reference 8 test (a factor of 5 lower than the Reynolds number of this test). The lower Reynolds number probably induced flow separation in the reference 8 test (the schlieren pictures given in that paper seem to indicate very extensive separation). This can result in large increases in static stability (see, e.g., ref. 9). However, the cross-sectional area of the base flare exposed to the air flow was 65 percent greater for the model of reference 8 than for the model of the present investigation. This, unfortunately, also contributes to the greater stability observed in reference 8 and makes it impossible to determine precisely the effect of the large change in Reynolds number.

Tests of the Hypersonically Similar Third-Stage Model

The test of the model hypersonically similar to the third-stage at a Mach number of 13.8 was conducted because the supersonic free-flight wind-tunnel facility was being modified at the beginning of this program and, therefore, it was possible to test only in the underground ballistic range. The intention of the test was to simulate Mach number 15 by applying the hypersonic similarity rule to the model to allow testing at a Mach number of 5. It was recognized that the application of the

hypersonic similarity rule to a blunt-nosed body is highly questionable.[2] Limited tests were made, however, and the results are compared with the geometrically similar third-stage results in figure 8.

In accordance with the similarity rule, the test results are presented for comparison as C_{m_α} vs. $M\alpha$. Now the Mach number simulated by the foreshortened hypersonically similar model is 13.8, and the test Mach number of the geometrically similar model is 9.6, so there remains a discrepancy in Mach number. However, this does not alter the conclusion that can be drawn. Note that the hypersonically similar model, with a rearward location of the center of gravity, is more stable than the geometrically similar model with a far-forward location of the center of gravity. Furthermore, the effect of increasing the Mach number on the geometrically similar model should be to reduce further the stability of that model, according to figure 5. Therefore, it can be seen that the hypersonically similar model gave results which do not quantitatively resemble the results from the geometrically similar model.

Boundary-Layer Separation

Since boundary-layer separation is known to affect the static stability of flare-stabilized bodies considerably (see, e.g., ref. 9), the following discussion will indicate the state of the boundary layer, separated or attached, and the probable influence of separation on the results of the present tests. The extent of boundary-layer separation at $M = 4$ on the third-stage model is shown in the shadowgraph of figure 9(a). The photograph shows the boundary layer to be laminar. The flow remained attached over most of the body with separation occurring near the body-flare juncture. The separated boundary layer reattached on the forward part of the flare and the main flare shock wave looks very much the same on the windward and sheltered sides. Angle of attack did affect separation slightly in that the separation point moved ahead on the lee side and aft on the windward side of the body. The separation point did not, however, move farther forward than 1-1/2 calibers ahead of the body-flare juncture. In one shadowgraph out of a total of fourteen the flow remained attached over the entire body (fig. 9(b)), indicating possibly that the conditions were close to critical for flow separation. We can only speculate as to the effect of flow separation on the stability. If the flow separates on the sheltered side only, there is produced an area of increased pressure on the sheltered side of the body just ahead of the flare, and this would act to decrease the restoring pitching moment.

[2]The assumptions made in developing the hypersonic similarity rule allow it to be used rigorously only when the body is slender and the flow is hypersonic. A blunt-nosed body violates the requirements of slenderness and, because the bow shock wave is detached, there exists a region of transonic rather than hypersonic flow.

It is believed, however, that since the flow deflection angle due to separation is small and the flow attached on the forward part of the flare, C_{m_α} was not greatly affected.

For the third-stage model flights near Mach number 10, no separated flow was observed on the shadowgraph negatives. The flow also remained attached on the second-stage configuration for the test conditions investigated.

The shadowgraphs of the hypersonically similar model show that the boundary layer is turbulent, and at small angles of attack (fig. 10(a)), the flow is attached. At large angles of attack (e.g., fig. 10(b)) the boundary layer separates on the sheltered side and the separation point moves forward as the angle of attack is increased. The pressure coefficient in this separated region, while higher on the cylinder ahead of the flare, is considerably lowered on the flare itself, and the net effect is believed to be an improvement in static stability. The fact that the boundary layer did not remain attached on the hypersonically similar model but did remain attached at comparable angles of attack on the third-stage model at $M = 9.6$ is a contributing reason why hypersonic similarity did not occur.

CONCLUDING REMARKS

As a result of these tests with a small-scale flare-stabilized body with hemisphere nose at Mach numbers from approximately 4 to 10, certain effects of Mach number and pitching amplitude on static longitudinal stability have been observed. The models tested were of the X-17 research test vehicle but the characteristics observed are thought to be typical of blunt-nosed flare stabilized bodies at hypersonic speeds.

Static longitudinal stability was found to decrease considerably with increasing Mach number. This decrease was due, in part at least, to the substantial decrease in dynamic pressure behind the strong bow shock wave with increasing Mach number.

The static longitudinal stability was also found to decrease markedly with decreasing pitching amplitude. Tests of the third-stage model at a Mach number of 9.8 indicated static instability for pitching amplitudes near zero. This phenomenon may also be attributed to the bow shock wave as explained in the text.

Tests made with the third-stage model showed a decrease in zero-lift drag coefficient with increasing Mach number. This decrease in drag is consistent with the observed decrease in static stability and may also be attributed to the reduction in dynamic pressure behind the strong bow shock wave with increasing Mach number.

Tests made with hypersonically similar models at low Mach numbers were found to be inapplicable in predicting static stability at high Mach numbers.

Ames Research Center
National Aeronautics and Space Administration
Moffett Field, Calif., Sept. 22, 1959

REFERENCES

1. Ross, F. W., and Dorrance, W. H.: An Introduction to a Supersonic Body Developmental Study. Engr. Res. Ctr., Univ. of Mich., UMM-40, Dec. 1949.

2. Kirk, Donn B., and Chapman, Gary T.: The Stabilizing Effectiveness of Conical Flares on Bodies With Conical Noses. NASA TM X-30, 1959.

3. Seiff, Alvin: A Free-Flight Wind Tunnel for Aerodynamic Testing at Hypersonic Speeds. NACA Rep. 1222, 1955.

4. Seiff, Alvin: A New Method for Computing Drag Coefficients From Ballistic Range Data. Jour. Aero. Sci., Readers' Forum, vol. 25, no. 2, Feb. 1958, p. 133.

5. X-17 Re-entry Test Vehicle R-10 Final Flight Report. Lockheed Aircraft Corp., MSD-3030, 1957.

6. X-17 Re-entry Test Vehicle D-6 Final Flight Report. Lockheed Aircraft Corp., MSD-1986, 1956.

7. Seiff, Alvin, Sommer, Simon C., and Canning, Thomas N.: Some Experiments at High Supersonic Speeds on the Aerodynamic and Boundary-Layer Transition Characteristics of High-Drag Bodies of Revolution. NACA RM A56I05, 1957.

8. Penland, Jim A., and Carroll, C. Maria: Static Longitudinal and Lateral Stability Parameters of Three Flared-Skirt Two-Stage Missile Configurations at a Mach Number of 6.86. NACA RM L57D15, 1957.

9. Dennis, David H., and Syvertson, Clarence A.: Effects of Boundary-Layer Separation on Normal Forces and Center of Pressure of a Cone-Cylinder Model With a Large Base Flare at Mach Numbers From 3.00 to 6.28. NACA RM A55H09, 1955.

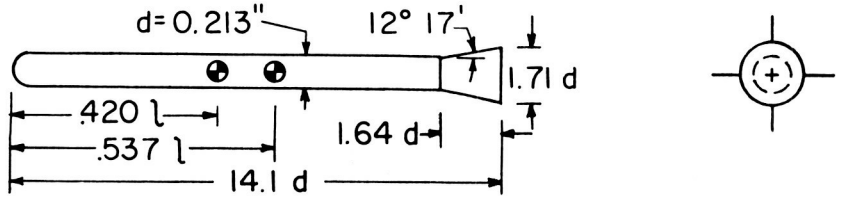

(a) Third-stage model.

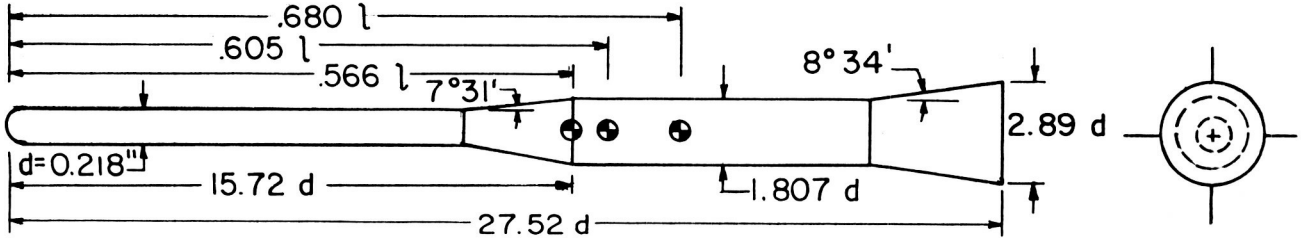

(b) Second-stage model.

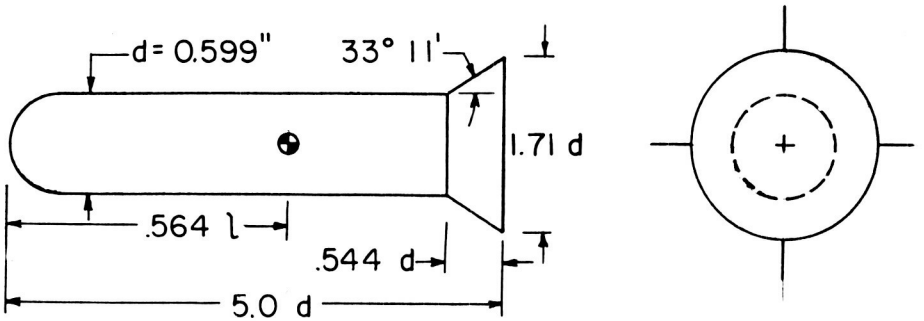

(c) Hypersonically similar third-stage model.

Figure 1.- Sketch of test models.

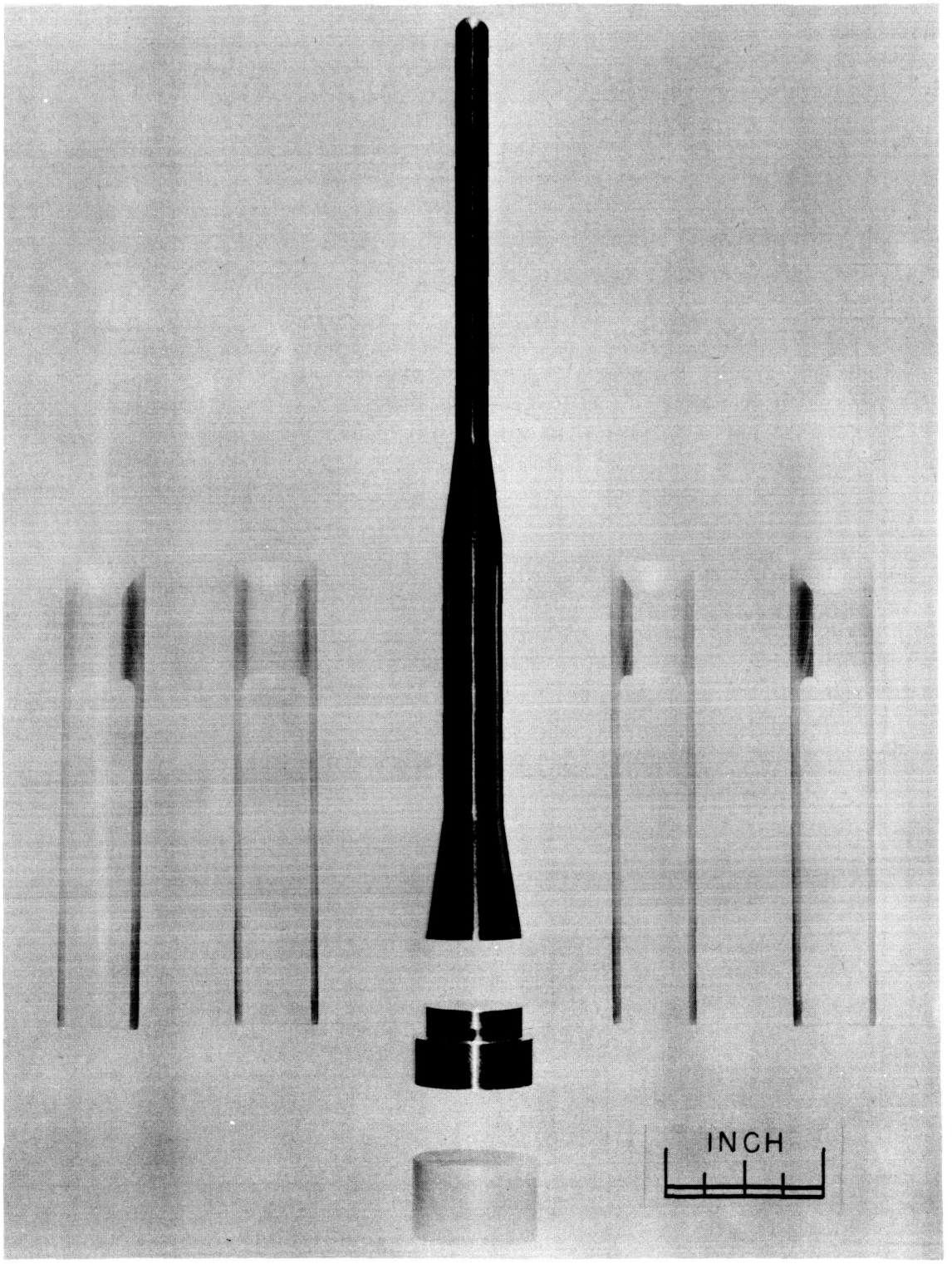

A-24347

Figure 2.- Photograph of second-stage model and sabot.

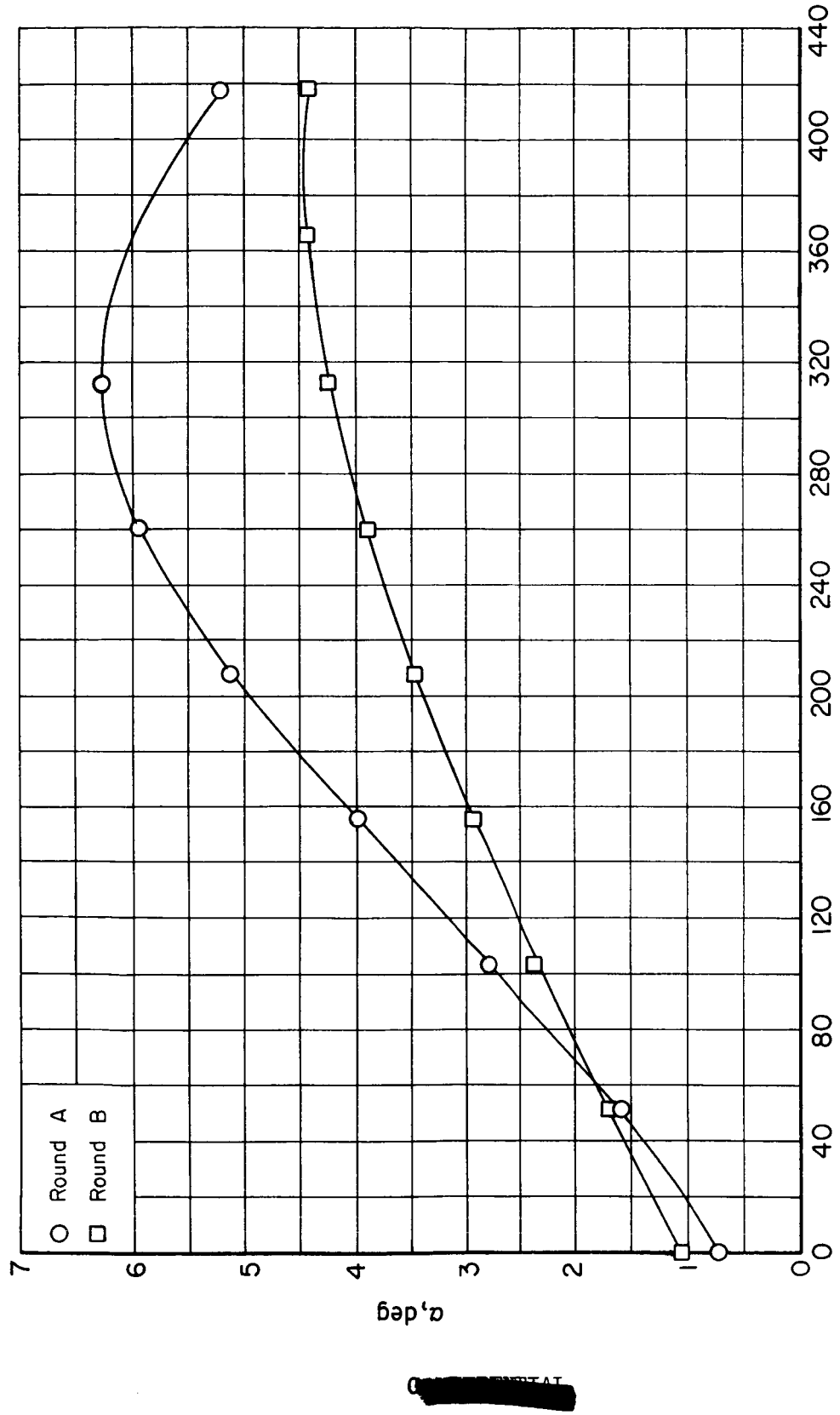

Figure 3.- Variation of angle of attack with x distance traveled for the third-stage configuration with X_{cg} = 0.420 l at Mach number 9.6.

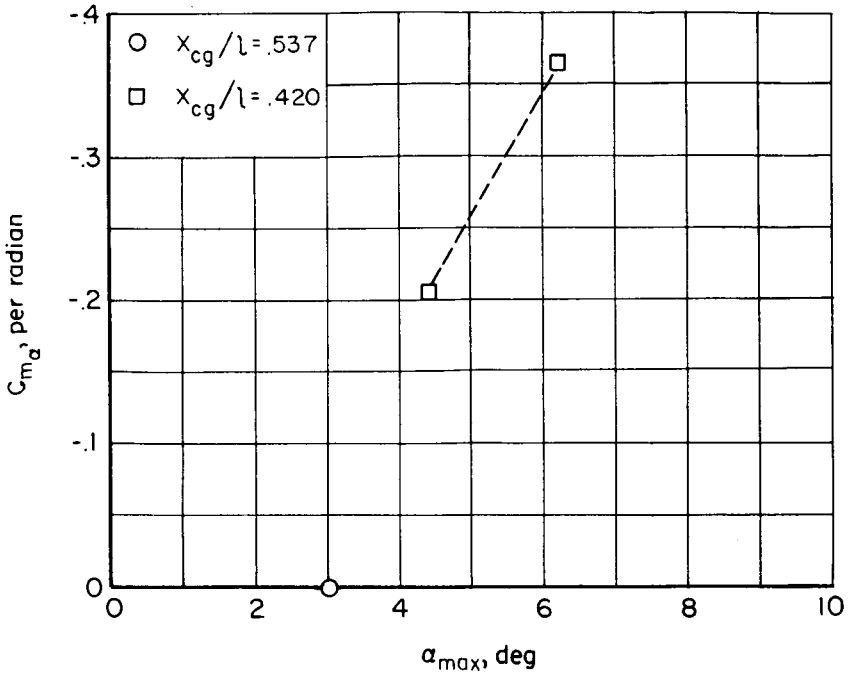

Figure 4.- Variation of effective C_{m_α} with maximum pitching amplitude for the third-stage configuration at $M \approx 9.6$.

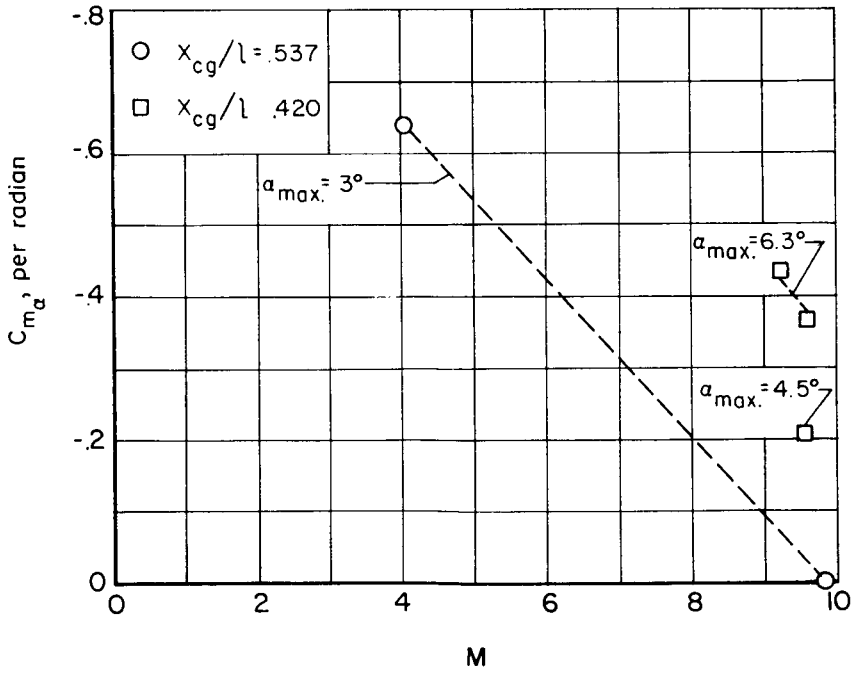

Figure 5.- Effect of Mach number on effective C_{m_α} for the third stage with two center-of-gravity locations.

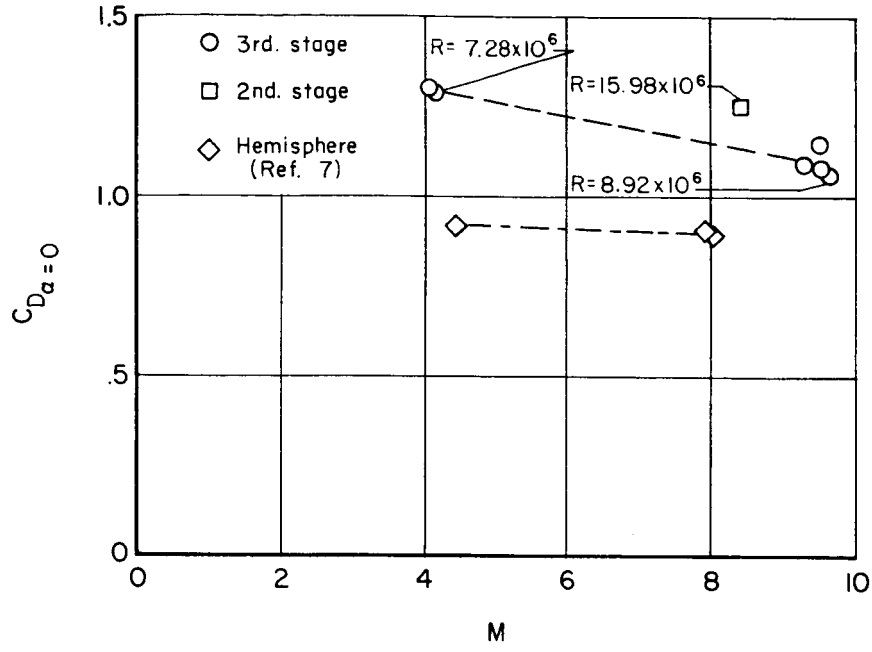

Figure 6.- Effect of Mach number on total zero-lift drag.

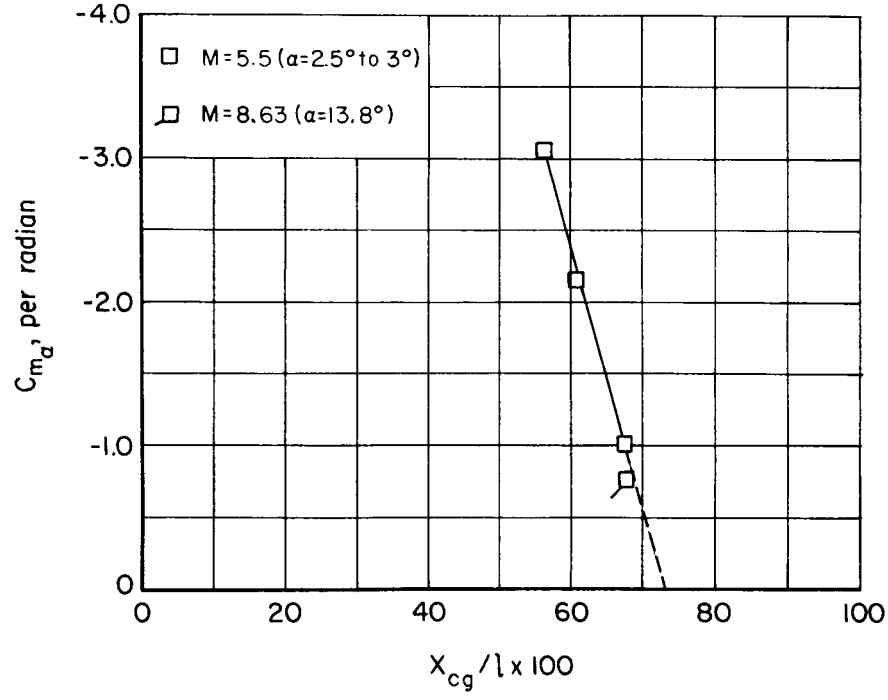

Figure 7.- Method used to determine values of center of pressure and effective normal-force-curve-slope coefficient.

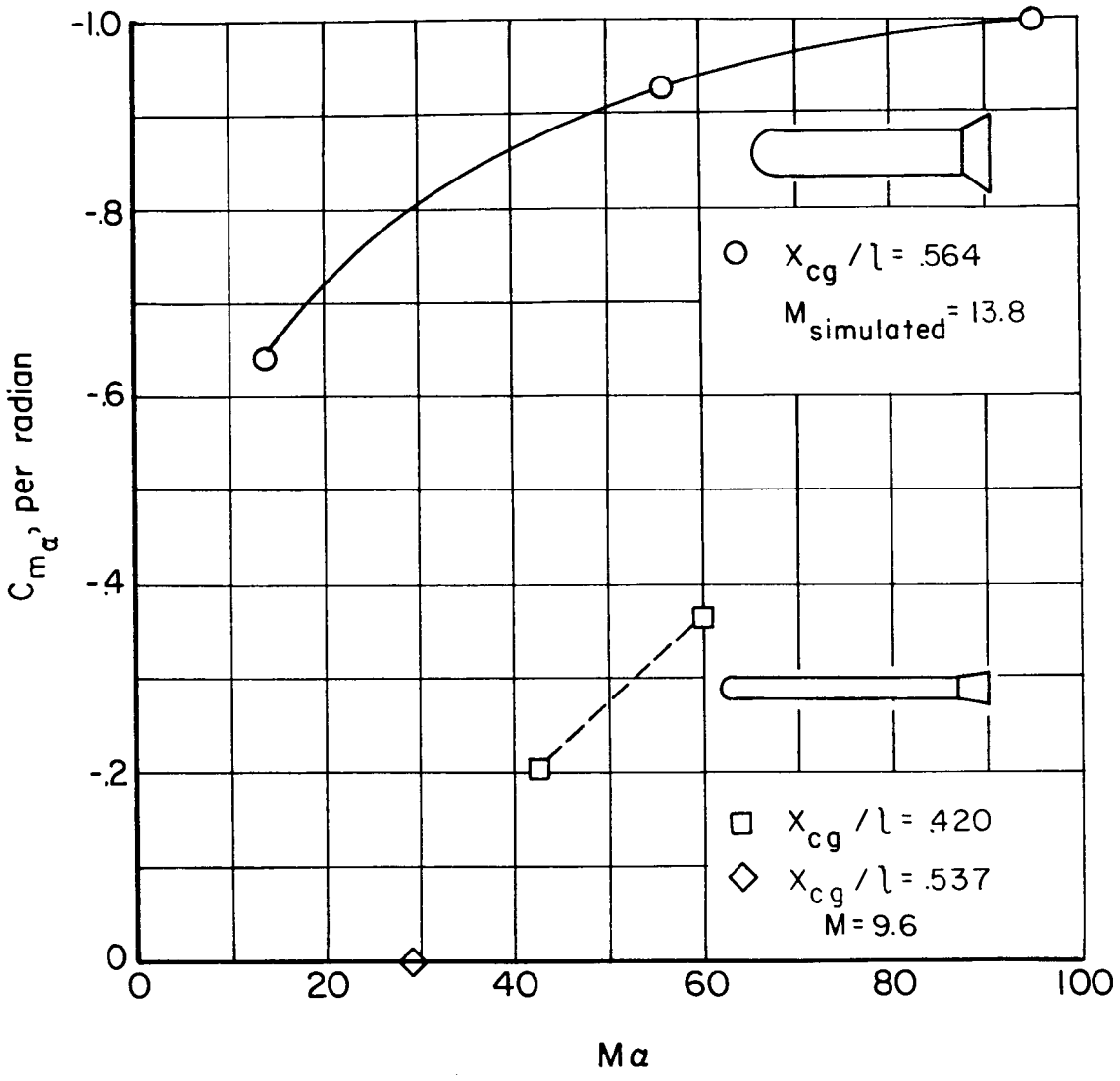

Figure 8.- Comparison of effective C_{m_α} for the hypersonically similar and third-stage configurations.

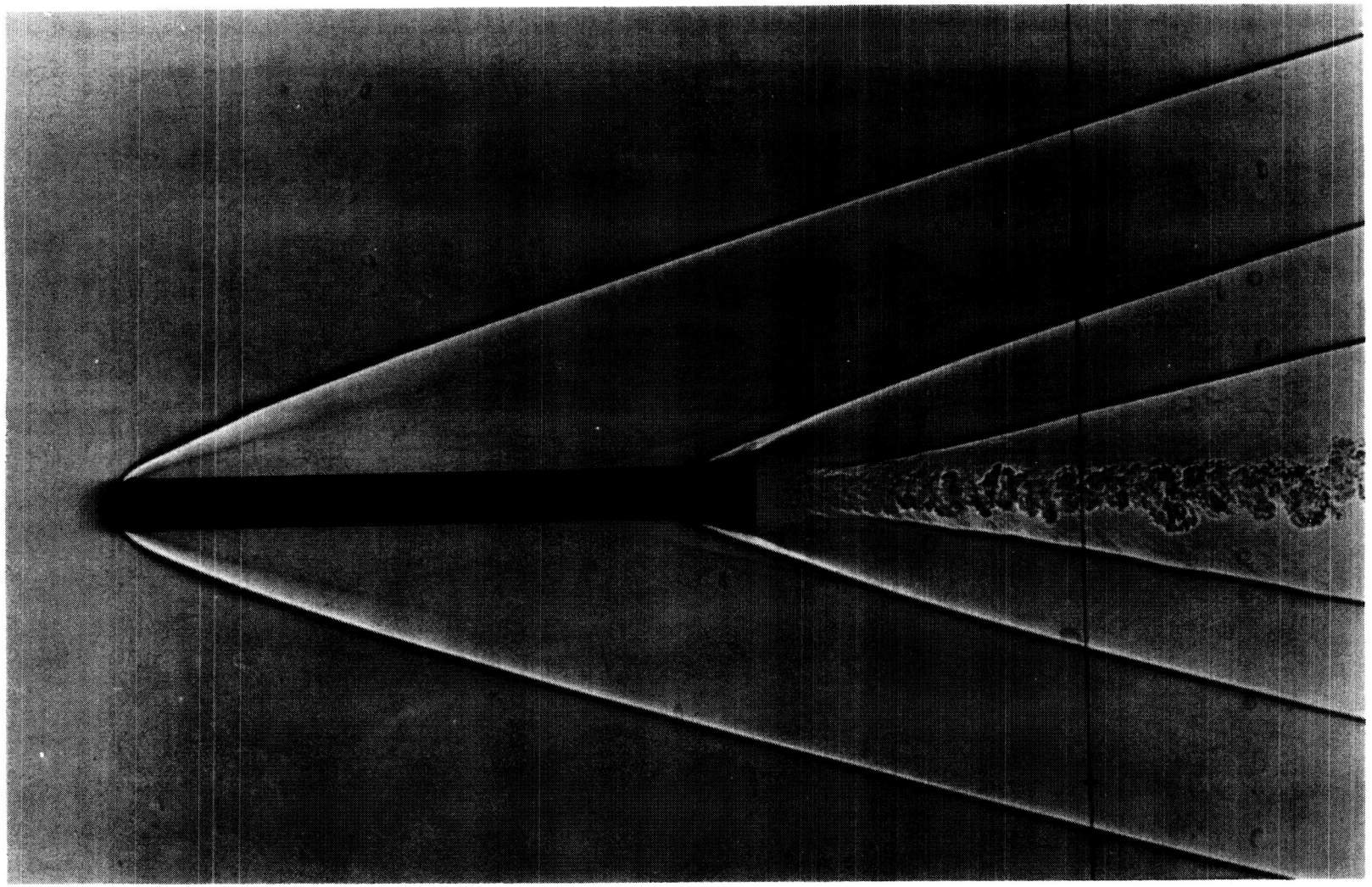

(a) Separated boundary layer.

Figure 9.- Shadowgraphs of third-stage configuration at $M = 4$ and $R = 7.3 \times 10^6$.

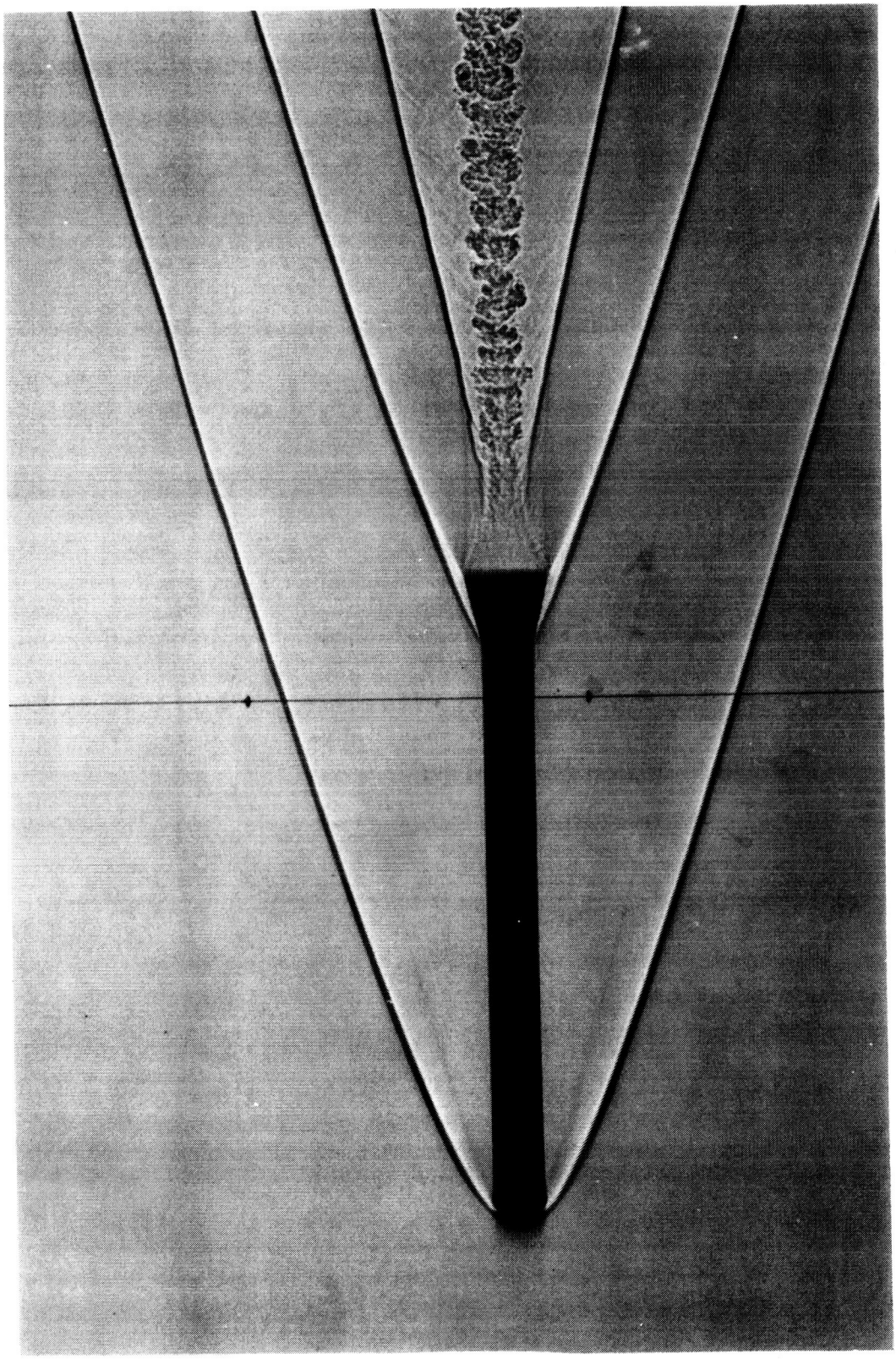

(b) Attached boundary layer.

Figure 9.- Concluded.

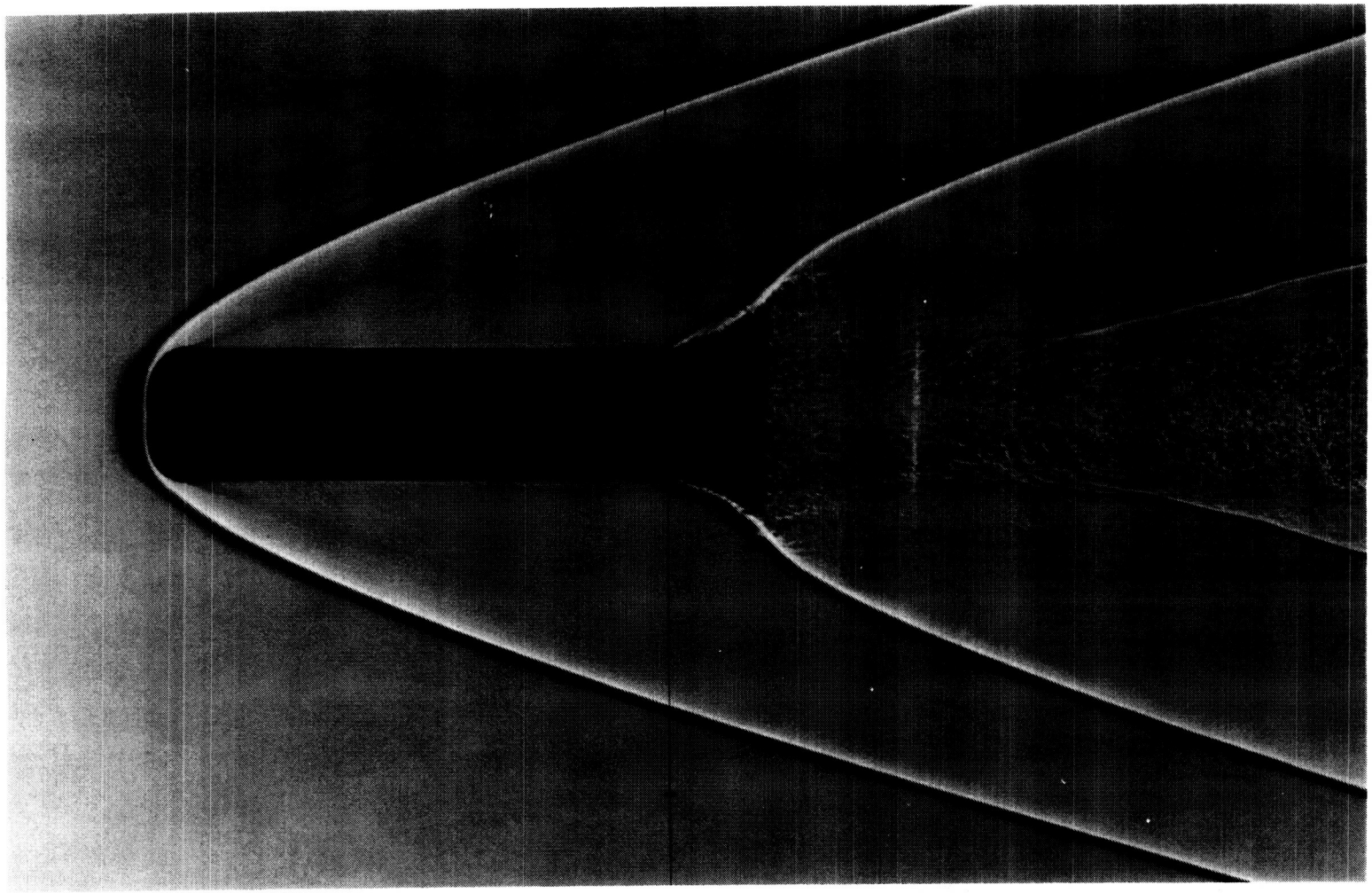

(a) $\alpha = 1\text{-}1/2^{\circ}$

Figure 10.- Shadowgraphs of the hypersonically similar third-stage model at $M = 4.7$ and $R = 8.3 \times 10^{6}$.

[redacted]

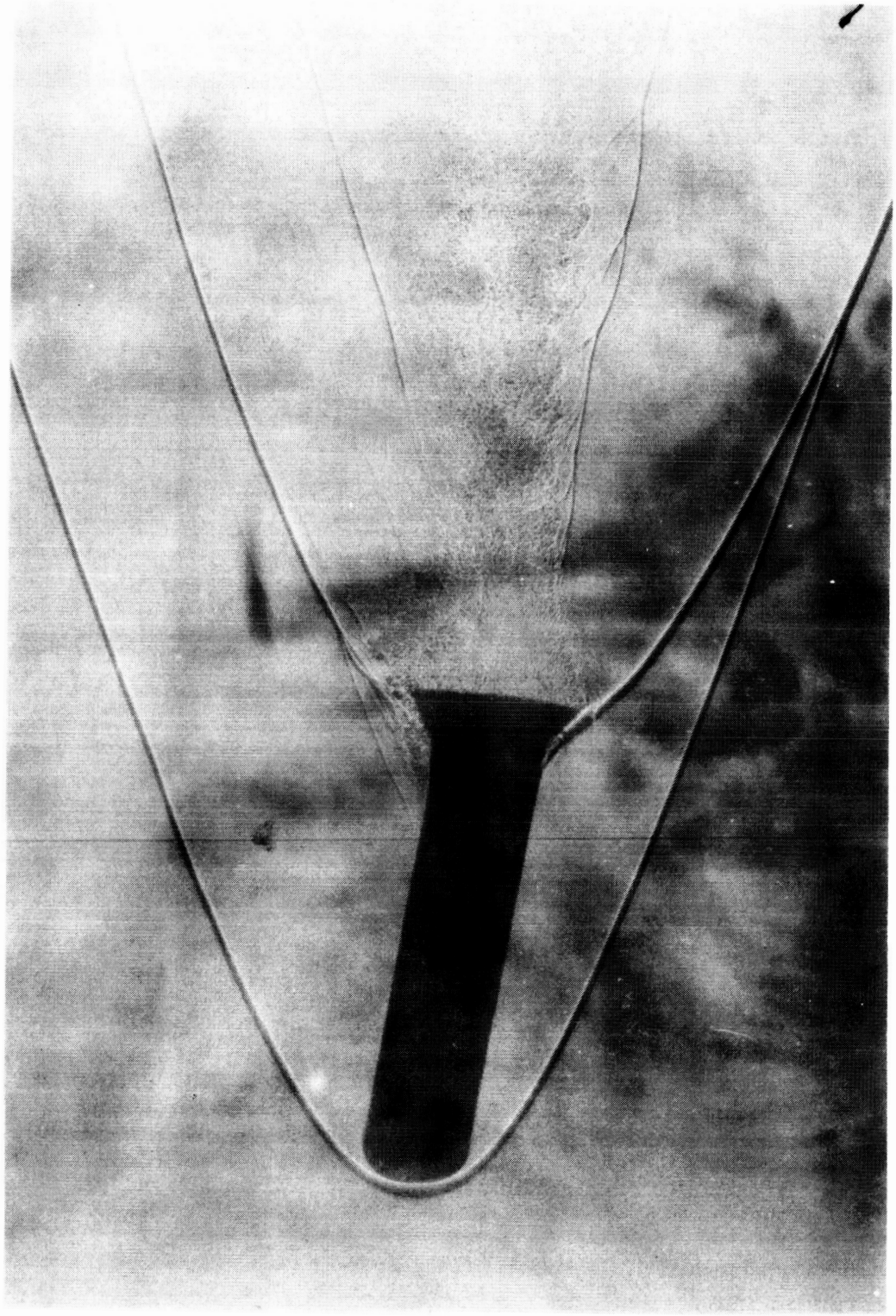

(b) $\alpha = 15^\circ$

Figure 10.- Concluded.